Macromolecules

pubs.acs.org/Macromolecules Article

Inducing Chiral Response in Conjugated Polymers Composed of Achiral Monomers Using Chiral End Groups

Siebe Detavernier, Trijntje Paredis, Silvia Pratesi, Julien De Winter, Elisabetta Salatelli, Pascal Gerbaux, and Guy Koeckelberghs*

Cite This: *Macromolecules* 2024, 57, 11229−11241 Read Online

ACCESS | Metrics & More | Article Recommendations | Supporting Information

ABSTRACT: Chiral expression in conjugated polymers is commonly achieved through the incorporation of stereogenic carbon atoms into the side chains of the polymer backbone. In this study, we explore the potential of inducing chiral expression in conjugated polymers by introducing chiral end groups via isolated external chiral initiators despite the presence of achiral side chains in the poly(3-octylthiophene) backbone. Two classes of chiral end groups are investigated: stilbene derivatives containing stereogenic carbon atoms in their side chains and (*S*)-(−)-1,1′-bi(2-naphthol) derivatives that exhibit axial chirality. Through solvatochromism experiments combined with UV−vis and circular dichroism (CD) spectroscopies, we identified the conditions necessary to induce chiral expression during supramolecular polymer aggregation.

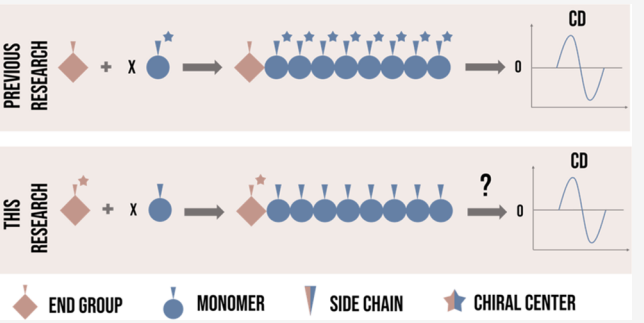

INTRODUCTION

In the last few decades, conjugated polymers (CPs) have gained significant attention due to their remarkable optical and electronic properties, making them suitable for various applications. These applications include organic photovoltaics (oPVs), organic field-effect transistors (oFETs), organic light-emitting diodes (oLEDs), chemical sensors, drug delivery systems, and the field of thermo-electrics (TE).[1−9] When these materials are implemented in such a broad range of applications, the actual characteristics of the polymer material must be tailored to optimize the performance. More specifically, device performance is strongly correlated with both the molecular and supramolecular structures, highlighting the importance of understanding and controlling them to create reproducible, tailor-made materials.[10−12] Regarding the molecular structure, the choice of monomer(s) alters the highest occupied molecular orbital (HOMO) and the lowest unoccupied molecular orbital (LUMO) levels of the resulting CPs, thereby influencing the bandgap of the polymer. Additionally, several parameters can be adjusted to change the supramolecular aggregation, including the degree of polymerization (DP), the backbone planarity, the nature of the side chains, the dispersity, the presence of defects, and even the choice of the end groups of the polymer material.[13−20] These factors can dictate the prevalent supramolecular aggregation types, i.e., type I (herringbone-like structure) and type II (comb-like structure) aggregation, which are important depending on the envisioned application.[21]

A frequently overlooked parameter is the nature of the end groups. End groups were once considered of minor importance because they were assumed to reside in the amorphous phase without influencing the aggregation behavior.[22] However, recent research has indicated that end groups are important for optimizing charge transport. For instance, the presence of phenyl-based end groups in an alternating copolymer of dithienogermole and 2,1,3-benzothiadiazole improves the charge-carrier mobilities by 1 order of magnitude compared to the analogue with hydrogen atoms as end groups.[23]

In addition, chiral expression of CPs using circular dichroism (CD) spectroscopy provides more insights into the aggregation behavior and the influence of end groups on polymer materials.[19,24] Chirality is typically introduced via a stereogenic carbon atom in the side chain of the monomers. CD and UV−vis spectroscopies have shown that both the nature and the bulkiness of the end groups impact the chiral aggregation behavior of CPs.[25,26] Overall, there is substantial evidence that the end groups significantly influence aggregation behavior rather than merely reside in the amorphous phase.

Nevertheless, the extent of their impact on the chiral expression of CPs remains unclear. This raises the fundamental

Received: August 28, 2024
Revised: November 14, 2024
Accepted: November 19, 2024
Published: November 27, 2024

https://doi.org/10.1021/acs.macromol.4c02054
Macromolecules 2024, 57, 11229−11241

Scheme 1. Overview of the Synthesis of the Stilbene-Derived External Initiators with Chiral (*S*)-2-Methylbutoxy or Achiral Butoxy Side Chains, based on Methyl Gallate (4a−b) (Top) or Hydroquinone (13a−b) as the Starting Material (Bottom)[a]

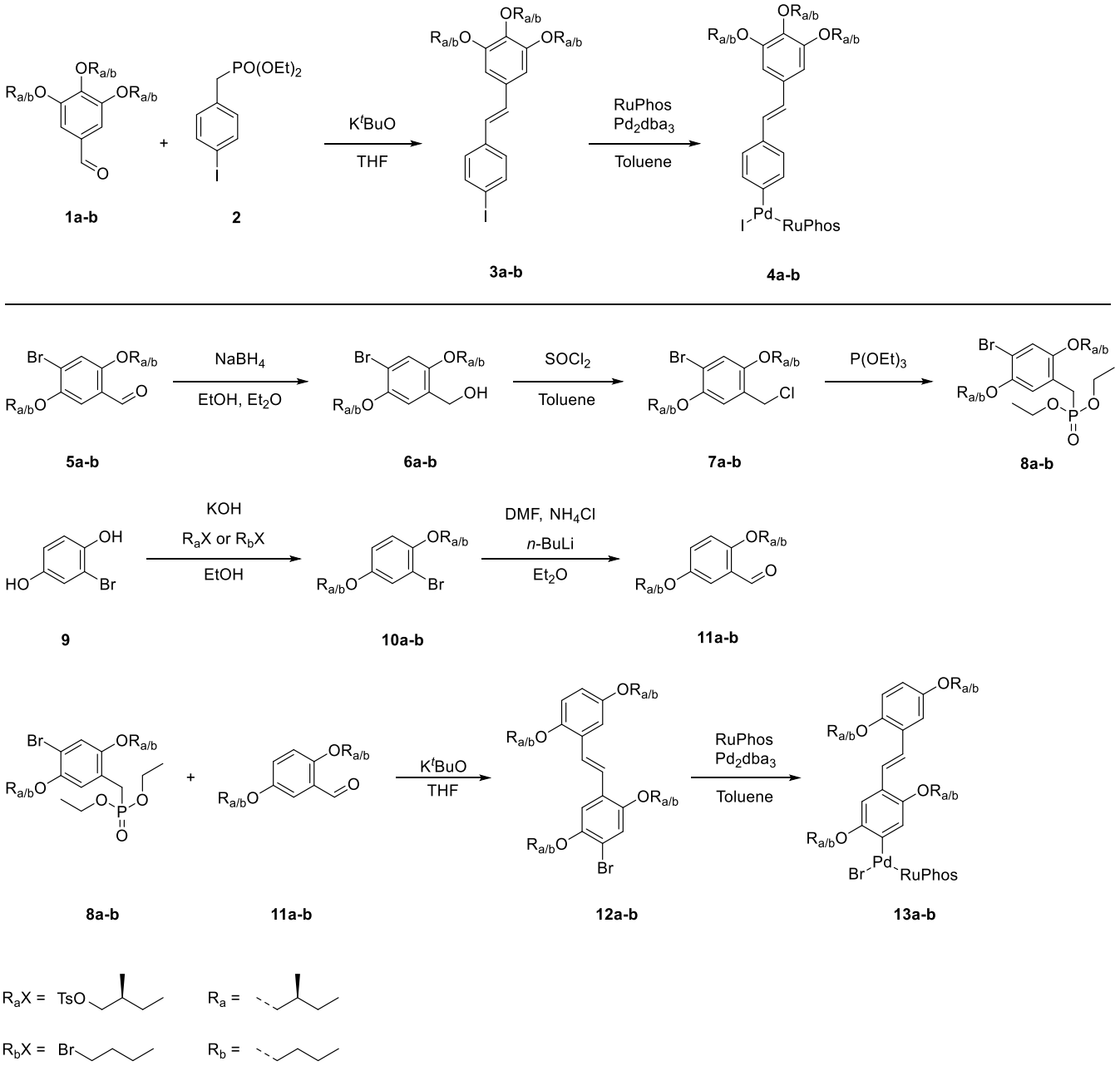

[a]dba = Dibenzylideneacetone and RuPhos = 2-dicyclohexylphosphino-2′6′-diisopropoxybiphenyl.

question of whether incorporating chiral end groups in an achiral CP may trigger chiral supramolecular aggregation and what conditions the end group must meet to achieve this effect. Furthermore, the difference in chiral expression of these CPs, synthesized from a chiral end group and achiral 3-alkylthiophene monomer repeating units, and chiral poly(3-alkylthiophene)s (P3ATs), synthesized from chiral monomers, is unknown. The aim is to synthesize polymers that operate via the sergeant and soldiers principle, where a small number of chiral entities, in this case just one, induces a chiral response throughout the rest of the achiral polymer system.[27−30] In this study, chiral end groups are introduced via chiral PdRuPhos initiators (RuPhos = 2-dicyclohexylphosphino-2′,6′-diisopropoxybiphenyl) using chain-growth Suzuki−Miyaura catalyst transfer condensative polymerizations (SMCTCP). This polymerization method is preferred as it tolerates various functional groups and is less prone to irreversible trapping on certain monomers or end groups compared to Kumada CTCP using Ni initiators.[31−33] This approach is motivated by recent advances that have improved the controlled character of the SMCTCP.[34−37] Additionally, aryl-PdRuPhos-halide initiator molecules are air- and water-stable, can be kept in solution longer than Ni initiators, and are compatible with a wide range of aryl halides.

Two classes of chiral end groups are proposed: (i) stilbene-derived end groups with chiral alkoxy side chains and (ii) (*S*)-(−)-1,1′-bi(2-naphthol)-derived (BINOL) end groups. The stilbene-derived end groups, with their stereogenic carbon

https://doi.org/10.1021/acs.macromol.4c02054
Macromolecules 2024, 57, 11229−11241

Scheme 2. Overview of the Synthesis of Propylene (16) and Methylene (18) Linked BINOL-Derived External Initiators and the Unlinked, with Two Methoxy Groups, (20) BINOL-Derived External Initiators Based on (*S*)-(−)-1,1′-Bi(2-naphthol)[a]

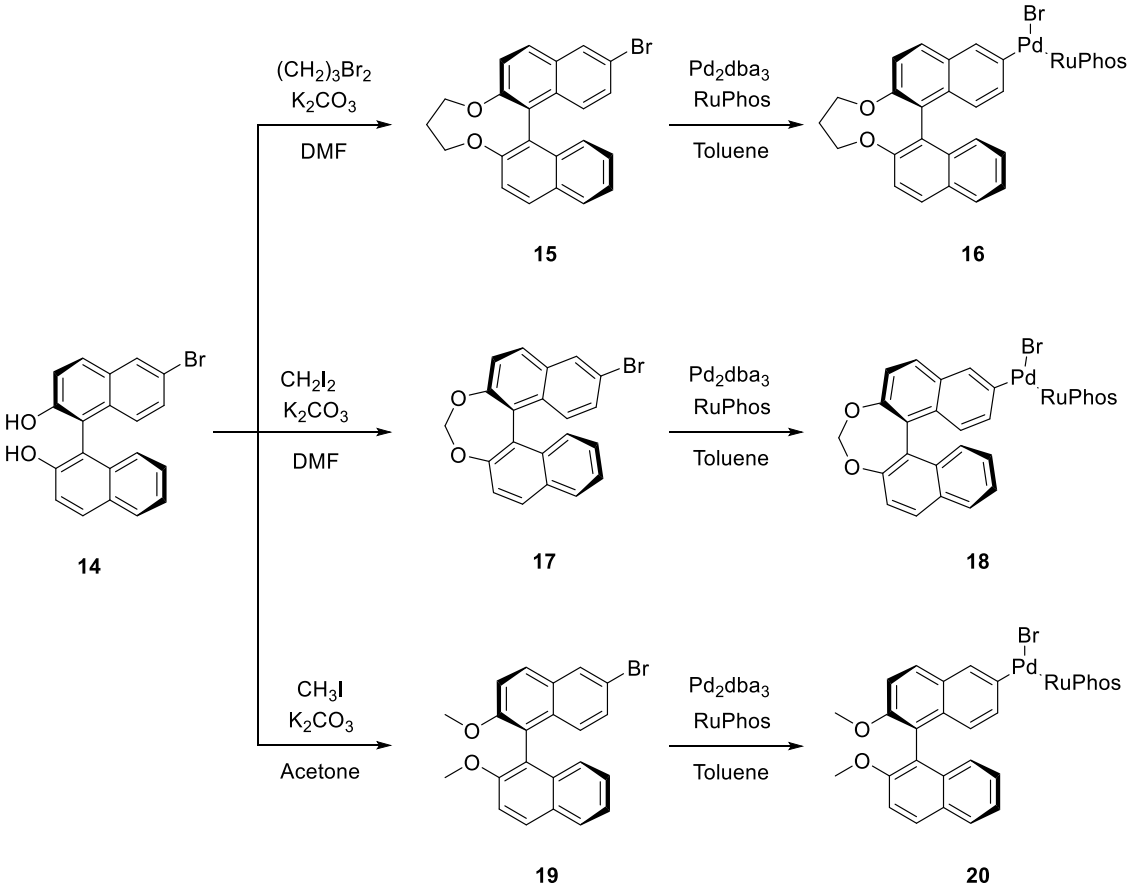

[a]dba = Dibenzylideneacetone, and RuPhos = 2-dicyclohexylphosphino-2′,6′-diisopropoxybiphenyl.

atoms, vary in the position of the chiral alkoxy side chains, thereby altering the distance and orientation of the chiral substituents relative to the polymer's side chains. The DP is also varied with a small number of monomer units to investigate if the influence of the end group diminishes with increasing chain length. The BINOL-derived end groups achieve chirality from a hindered rotation around the single bond between the two naphthol units, leading to a nonplanar arrangement and axial chirality. This atropisomer can be modified via an extra coupling between the two naphthol groups with different alkyl linkers to alter the dihedral angle, rigidity, and bulkiness.[38,39] After the introduction of the end group utilizing the external initiator and further polymerization, the obtained polymers are characterized to verify end group fidelity. Subsequently, they are used in solvatochromism experiments, where the chiral supramolecular aggregation behavior is investigated using UV−vis and CD spectroscopies.

RESULTS AND DISCUSSION

First, the possibility of inducing chiral aggregation in otherwise achiral CPs and the conditions required from the end group to obtain this effect are investigated. As mentioned before, different chiral end groups, i.e., stilbene and BINOL derivatives, are synthesized. The chiral stilbene derivatives vary in distance and orientation of the chiral side chains relative to the (achiral) side chains in the polymer backbone (Scheme 1). For the BINOL derivatives, the dihedral angle of the end group is modified by utilizing different linkers connecting the two naphthol functionalities to investigate the rigidity and bulkiness as parameters for chiral aggregation (Scheme 2).

During polymerization, specific end groups can be introduced at the initiation step or the termination step. It is preferred to introduce the end group during initiation to obtain a uniform material in which every polymer chain includes the chiral end group. This approach has two advantages: first, initiating at high efficiency is easier than achieving high-end-capping conversions during termination, as there is a possibility of side reactions after a higher number of monomer insertions. Second, the monomer-to-initiator ratio is used to govern the DP, and in the case of a controlled SMCTCP, every initiator molecule initiates exactly one polymer chain, reducing the (expensive) chiral end group consumption. In contrast, adding an end group during termination requires a significant excess to ensure high conversion and fast termination. Importantly, when using SMCTCP, the most efficient initiator molecules are currently synthesized *in situ* from G3 PdRuPhos in combination with an aryl iodide, resulting in an aryl-Pd(II)RuPhos-halide.[34] However, as these oxidatively inserted aryl-Pd(II)RuPhos-halide complexes are stable, they can be isolated to further enhance the overall control during the SMCTCP. Therefore, all of the Pd initiators are first synthesized and isolated before polymerization.

https://doi.org/10.1021/acs.macromol.4c02054
Macromolecules 2024, 57, 11229−11241

Scheme 3. Overview of the SMCTCP of Achiral M1 Using Chiral External Initiators for the Synthesis of Chiral End-Capped P3OTs[a]

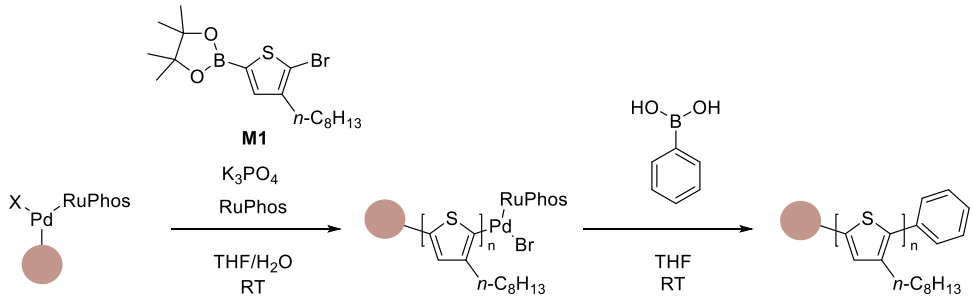

[a]With "brown circle solid" being the chiral stilbene or BINOL-derived aromatic compounds. RuPhos = 2-dicyclohexylphosphino-2′,6′-diisopropoxybiphenyl.

Table 1. Overview of the SMCTCP of Achiral M1 Using Chiral External Initiators for the Synthesis of Chiral End-Capped Polymers[a]

polymer	Pd initiator	monomer	M/I	time	$\bar{M}_n$[b] (kg/mol)	$Đ$[b]	DP	MM[c] (kg/mol)	$\frac{\bar{M}_n}{MM}$[c]
STILB GALL*-P3OT$_{30}$	**4a**	**M1**	30	21 h	8.7	1.25	30	6.3	1.38
STILB HQ*-P3OT$_{28}$	**13a**	**M1**	30	6 h	7.2	1.23	28	6.0	1.20
BINOL P*-P3OT$_{33}$	**16**	**M1**	30	3 h	7.2	1.24	33	7.2	1.07
BINOL M*-P3OT$_{39}$	**18**	**M1**	30	3 h	9.0	1.31	39	9.0	1.14
BINOL 2xMe*-P3OT$_{33}$	**20**	**M1**	30	4 h	7.4	1.28	33	7.4	1.10
STILB HQ*-P3OT$_{25}$	**13a**	**M1**	30	5 h	6.7	1.17	25	5.4	1.24
STILB HQ*-P3OT$_{23}$	**13a**	**M1**	30	5 h	5.4	1.22	23	5.0	1.08

[a]M/I: monomer-to-initiator ratio used to determine the theoretical DP. [b]$\bar{M}_n$ and $Đ$ are determined via SEC measurements. [c]DP and MM (molar mass) are determined via ^{1}H NMR.

For the first class of initiators, four different stilbene-derived aryl halogenides are synthesized: two chiral ones, 5-((*E*)-4-iodostyryl)-1,2,3-tri((*S*)-2-methylbutoxy)benzene **3a** and 1-((*E*)-2,5-di((*S*)-2-methylbutoxy)styryl)-4-bromo-2,5-di((*S*)-2-methylbutoxy)benzene **12a**, as well as their achiral counterparts, (*E*)-1,2,3-tributoxy-5-(4-iodostyryl)benzene **3b** and (*E*)-1-bromo-2,5-dibutoxy-4-(2,5-dibutoxystyryl)benzene **12b** (Scheme 1). The synthesis starts from the corresponding commercially available products methyl gallate and hydroquinone. A relatively short side chain, (*S*)-2-methylbutoxy, is preferred for easier purification and improved aggregation, in addition to the presence of a stereogenic carbon atom (Scheme 1, R$_a$). A butoxy side chain is used as the achiral equivalent (Scheme 1, R$_b$). For the synthesis of **3a** and **3b**, **1a** or **1b** and **2** are coupled using the Horner−Wadsworth−Emmons (HWE) reaction, which favors the *trans*-product. In the final step, Pd initiators **4a** (chiral) and **4b** (achiral) are obtained via the reaction of the aryl halides**3a** (chiral) or **3b** (achiral) with Pd$_2$dba$_3$ (dba = dibenzylideneacetone) and RuPhos as ligand in toluene. Ligand exchange and oxidative insertion in the carbon−halogen bond produce the aryl-Pd(II)RuPhos-halides. The crude mixture is concentrated and filtered over Celite to remove Pd(0) black and precipitated in pentane and diethyl ether (Scheme 1 and Supporting Information, Part 4). For initiators **13a** (chiral) and **13b** (achiral), the stilbene derivative is synthesized from two hydroquinone-based units with different functional groups. The first hydroquinone **5a−b** is reduced with NaBH$_4$, converted from alcohol to chloride with SOCl$_2$, and finally reacted with triethyl phosphite to form phosphonate **8a−b**. For the second ring in the stilbene derivative, 2-bromohydroquinone is used as the starting material, followed by alkylation with either chiral (*S*)-2-methylbutyl *p*-toluenesulfonate for the synthesis of **10a** or achiral 1-bromobutane for the synthesis of **10b**. Next, a Bouveault reaction with *n*-butyllithium and dimethylformamide affords aldehyde **11a−b**. **13a** (chiral) and **13b** (achiral) are eventually obtained using similar HWE reactions, e.g., **8a** (chiral) with **11a** (chiral) and **8b** (achiral) with **11b** (achiral), and following reaction with Pd$_2$dba$_3$ and RuPhos (Scheme 1 and Supporting Information, Part 4). All external initiators are characterized with ^{1}H, ^{13}C, and ^{31}P NMR (Supporting Information, Part 6).

For the second class, a similar PdRuPhos initiator is synthesized. (*S*)-(−)-1,1′-Bi(2-naphthol) is used as the starting material to obtain brominated product **14**. From **14**, the naphthol functionalities are coupled with either a propylene **15** or methylene **16** linker or left unlinked after etherification to two methoxy groups **17** (Scheme 2). After a similar reaction with Pd$_2$dba$_3$ and RuPhos, the external initiators are obtained. All initiators were found to be stable under ambient conditions and for several days in solution. Based on the dihedral angle of (*S*)-(−)-1,1′-bi(2-naphthol), the derivative with two methoxy groups **20** can be considered to have a similar dihedral angle of around 93°. The dihedral angle of the propylene-linked **16** reduces to a global minimum of 66° and methylene-linked **18** even further to 49°.[38] However, the rigidity of these three end groups varies during aggregation, as end group **20** can be more easily influenced than the other two BINOL end groups (**16** and **18**).

The first series of polymers are synthesized using SMCTCP (Scheme 3). As the monomer, achiral 2-(5-bromo-4-octylthiophen-2-yl)-4,4,5,5-tetramethyl-1,3,2-dioxaborolane **M1** is synthesized according to literature procedures (Supporting Information, Part 3). All of the polymers are

https://doi.org/10.1021/acs.macromol.4c02054
Macromolecules 2024, 57, 11229−11241

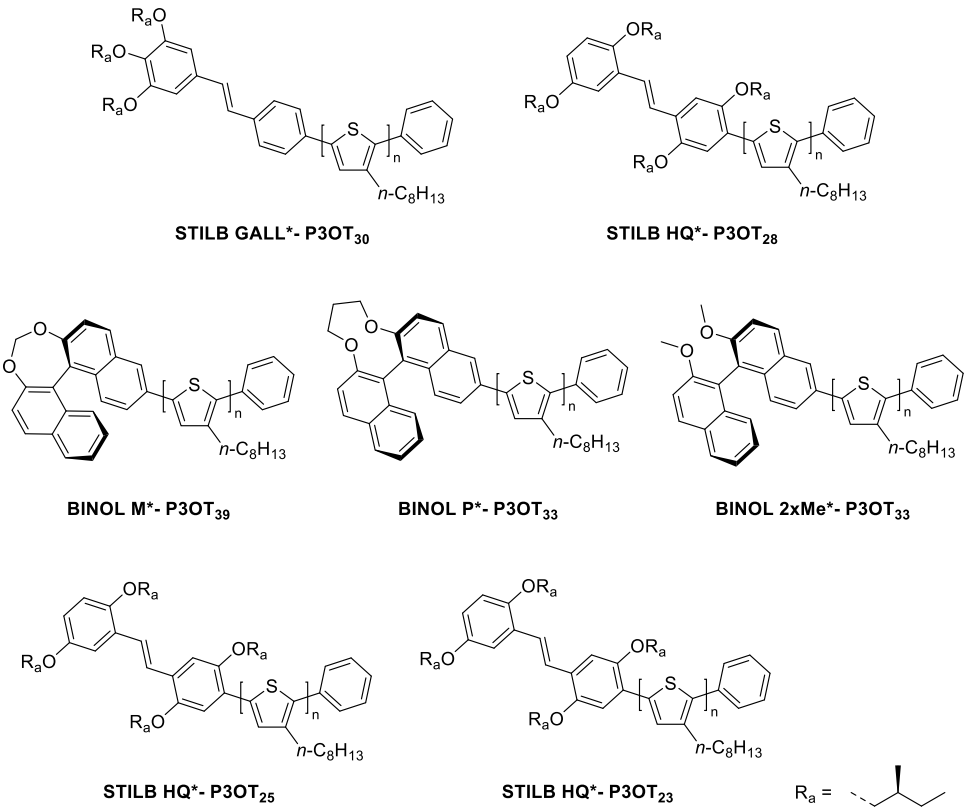

Figure 1. Overview of the first seven polymers synthesized. They all consist of a chiral end group and an achiral polymer backbone.

limited at a DP of 30 as this would (i) improve the share of the end group compared to the overall length of the polymer backbone and (ii) provide control over the polymerization and thus also the uniformity of the end groups.

Overall, a chiral external initiator, stilbene-derived (**4a** or **13a**) or BINOL-derived (**16**, **18** or **20**), in combination with achiral **M1**, is polymerized to form chiral end-capped poly(3-octylthiophene) (P3OT) using K_3PO_4 as a base and additional RuPhos as a ligand in a THF/H_2O solvent mixture (0.02 M, v/v 40/1) at room temperature. All parameters are kept constant during the different polymerizations except the reaction time (Table 1). The polymerizations are monitored by size-exclusion chromatography (SEC). The polymerization rate for the stilbene-initiated polymers is lower than the BINOL-initiated polymers, possibly due to the reversible trapping of the Pd moiety onto the C=C double bond of the stilbene moiety.[40] After full conversion, the polymerization is terminated with an excess of phenylboronic acid, and subsequently, the polymers are purified using Soxhlet extraction. The molar masses of the polymer samples are measured using SEC. Note that the molar mass based on SEC data is overestimated, as the calibration was obtained using poly(styrene) standards. Still, the molar mass gives an indication and can be used to compare the different samples. The following polymers are obtained: **STILB GALL*-P3OT$_{30}$**, **STILB HQ*-P3OT$_{28}$**, **BINOL P*-P3OT$_{33}$**, **BINOL M*-P3OT$_{39}$**, and **BINOL 2xMe*-P3OT$_{33}$** (all polymers are visualized in Figure 1), where **STILB GALL** and **STILB HQ** refer to stilbene end groups based on gallate and hydroquinone derivatives, respectively. For **BINOL M**, **P**, and **2xMe**, "**M**" indicates a methylene linker, **P** denotes a propylene linker, and **2xMe** refers to the unlinked BINOL. The "*" denotes the chiral part of the polymer, which in this series is always the end group, while the **P3OT$_{XX}$** polymer backbone is achiral. "$_{XX}$" refers to the DP as determined by integration from the ^{1}H NMR spectra.

In this first series, the samples with a stilbene-derived end group, **STILB GALL*-P3OT$_{30}$** and **STILB HQ*-P3OT$_{28}$** (Table 1), have decent dispersities, 1.25 and 1.23, respectively. The molar mass ranges from 8.7 to 7.7 kg/mol. For the different BINOL-initiated polymers, the dispersity is somewhat higher, ranging from 1.24 to 1.31, which might be related to a slower initiation due to the bulkiness of the end group. The $\bar{M}_n$ remains rather constant, except for **BINOL M*-P3OT$_{39}$**, which has a higher $\bar{M}_n$ of 9.0 kg/mol. Using ^{1}H NMR, the DP could be determined via the integration of one of the signals of the end group and the α-methylenes of the side chain on the polymer backbone. In order to do this, the presence and uniformity of the first end group in the polymer sample, obtained via initiation, are confirmed using matrix-assisted laser desorption/ionization time-of-flight (MALDI-ToF) mass spectrometry. From these spectra, it is clear that all polymer samples contain the desired end group inserted during initiation (Supporting Information, Part 8). As is the case, ^{1}H NMR is used to more accurately determine the DP of the polymer samples. This confirms that the targeted DP, based on the monomer-to-initiator ratio, is in close agreement with the DP based on the ^{1}H NMR spectra (Table 1). However, similar to the SEC measurement, **BINOL M*-P3OT$_{39}$** has a higher DP compared to that of the other samples.

The $\bar{M}_n$ from SEC data can be divided by the molar mass calculated from ^{1}H NMR by multiplying the molar mass of the repeating unit by the DP and adding the molar mass of the end group, which indicates the overestimation of SEC. For **STILB GALL*-P3OT$_{30}$** and **STILB HQ*-P3OT$_{28}$**, the molar masses based on ^{1}H NMR are 6.3 and 6.0 kg/mol, with SEC-to-NMR

https://doi.org/10.1021/acs.macromol.4c02054
Macromolecules 2024, 57, 11229−11241

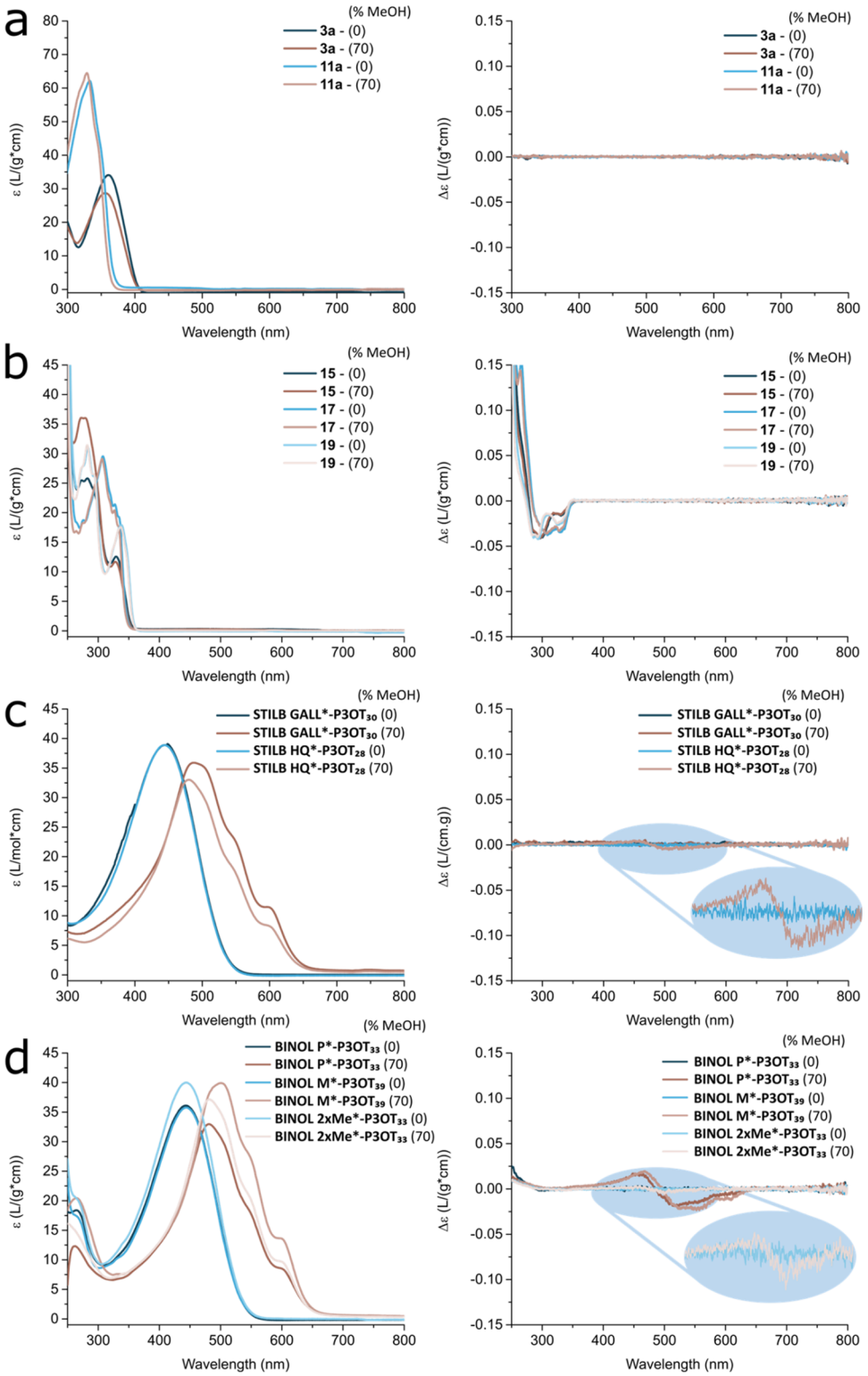

Figure 2. Absorption and CD spectra of the solvatochromism experiments of (a) the chiral stilbene end groups (aryl-Br, **3a**, and **12a**), (b) chiral BINOL end groups (aryl-Br, **15**, **17**, and **19**), (c) stilbene-derived polymers, and (d) BINOL-derived polymers. The blue spectra are samples measured in $CHCl_3$, whereas the brown spectra are under poor solvent conditions (70% MeOH).

ratios of 1.38 and 1.20, respectively (Table 1). The larger overestimation of **STILB GALL*-P3OT$_{30}$** is likely due to its more planar end group, which increases the hydrodynamic volume, whereas the position of **STILB HQ*-P3OT$_{28}$**'s side chains causes more steric hindrance and a less planar end group. The BINOL-derived polymers have lower ratios, below 1.14, due to the dihedral angle between the two naphthalenes, leading to a smaller hydrodynamic volume compared with the more rigid stilbene end groups and the polymer backbone.

Next, the self-assembly of the polymer materials is investigated via UV−vis and CD measurements to determine whether the chiral end group can induce the chiral aggregation

https://doi.org/10.1021/acs.macromol.4c02054
Macromolecules 2024, 57, 11229−11241

of the polymer backbone itself. Solvatochromism experiments are performed by dissolving the polymers in chloroform ($CHCl_3$), a good solvent where the individual polymer chains obtain a random coil-like structure. In this state, P3ATs with chiral side chains do not exhibit chiral expression. Subsequently, methanol (MeOH), a nonsolvent, is gradually added to the solution. This induces supramolecular aggregation, which typically results in the formation of a one-handed helically organized structure (M or P helix) in the case of P3AT with chiral side chains. Given that CD spectroscopy is highly sensitive, the conditions under which the measurements are performed were kept constant as much as possible. Measurements are conducted at room temperature, with the nonsolvent added using an automatic syringe at a rate of 0.175 mL/min while stirring the solution at a constant rate of 350 rpm and allowing the sample to equilibrate for 5 min. To ensure reproducibility and reliability, the measurements under poor solvent conditions are repeated twice. Nonsolvent is added until 70% of the total solvent volume consists of MeOH.

First, the individual precursors for the end groups, i.e., the aryl halides (**3a**, **12a**, **15**, **17**, and **19**), are examined to determine if they would aggregate under the proposed conditions and if they exhibit chiral expression. It is important to note that the Pd initiators themselves are not measured, as they differ significantly from the actual end groups due to the presence of Pd and the ligand. For the stilbene derivatives (Figure 2a), no distinct changes are observed between 0 and 70% MeOH in the UV−vis spectra. As expected from the UV−vis data, no chiral aggregation is observed. Similarly, for the three BINOL derivatives, no significant differences are observed in the UV−vis spectra (Figure 2b). However, the CD spectra already reveal chiral expression both in $CHCl_3$ (0% MeOH) and under poor solvent conditions (70% MeOH). The signal appears between 250 and 350 nm and does not significantly change under the different solvent conditions. This is likely because the end groups (**15**, **17**, and **19**) already possess a fixed chiral orientation around a single bond, making them CD-active, even without aggregation. The similarity in CD signal intensity among the BINOL derivatives suggests that their effects can be directly compared when introduced into the polymer backbone.

Next, the polymers based on achiral monomers (**M1**) and chiral end groups are measured. A clear distinction is observed for **STILB GALL*-P3OT$_{30}$** and **STILB HQ*-P3OT$_{28}$**, both featuring a stilbene end group (Table 1). As expected, no chiral expression is detected when **STILB GALL*-P3OT$_{30}$** and **STILB HQ*-P3OT$_{28}$** are dissolved in $CHCl_3$ and behave as individual chains. However, upon aggregation of the polymer chains into supramolecular structures, **STILB HQ*-P3OT$_{28}$** exhibited chiral aggregation, as evidenced by a small bisignate Cotton effect with zero-crossing around 479 nm (Figure 2c). This value corresponds to λ_{max} of the absorbance band of P3OT in the UV−vis spectrum, indicating that the polymer itself aggregates in a chiral manner. As the UV−vis and CD signals of the aggregated polymers appear at higher wavelengths than those of the end group itself, it can be concluded that the end group transfers its chirality onto the achiral polymer chain. The end group acts as the sole sergeant with the achiral polymer chain as soldiers being forced into a chiral supramolecular organization. In contrast, aggregation of **STILB GALL*-P3OT$_{30}$** did not yield a CD signal, although a red-shift due to planarization and polymer aggregation is observed in the UV−vis spectrum. This suggests that both the position and the orientation of the side chains are crucial for inducing chiral aggregation (Figure 3). The side chains of the

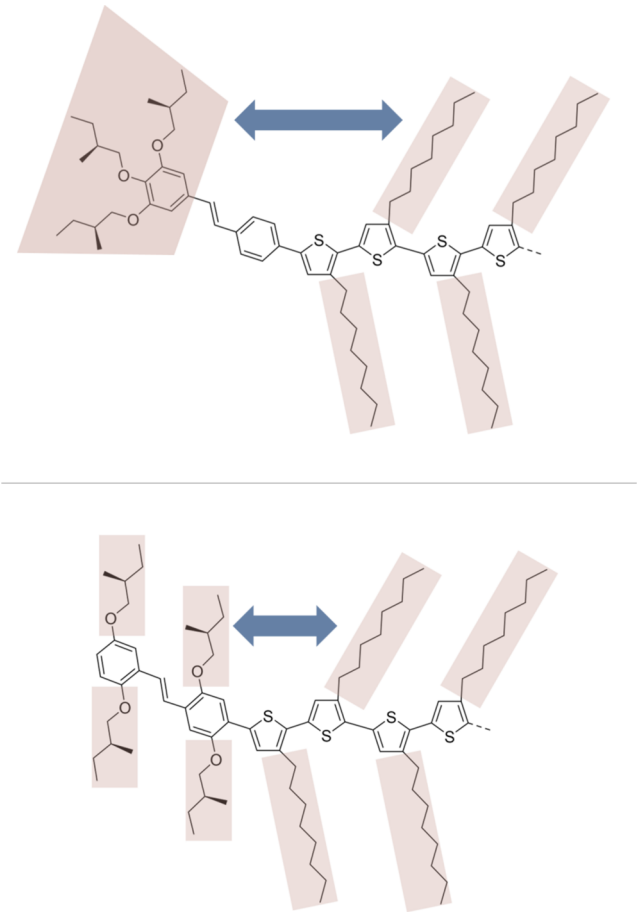

Figure 3. Distance (blue arrows) and orientation (pink quadrilaterals) of the side chains of the end group and the polymer backbone. Top: the distance is larger, and the side chains are pointing in different directions. Bottom: shorter distance and more parallel orientation between the side chains of the end group and the polymer backbone.

end group in **STILB GALL*-P3OT$_{30}$** are almost perpendicular to those in the polymer, and the distance between them is relatively large due to the presence of the unsubstituted aromatic ring near the P3OT. The combination of these two factors reduces the impact of the end group on the aggregation.

The same procedure is repeated for the polymers with BINOL-derived end groups. Upon aggregation, both **BINOL P* P3OT$_{33}$** and **BINOL M* P3OT$_{39}$**, with the propylene- and methylene-linked BINOL-derived end group, respectively, show a negative bisignate Cotton effect in the CD spectrum. The CD signal is again present in the absorption band of P3OT (Figure 2d). **BINOL 2xMe* P3OT$_{33}$**, which has an unlinked BINOL derivative, shows a significantly smaller CD signal. This indicates that the chiral expression is not solely dependent on the bulkiness of the end group but also on the dihedral angle and the rigidity, with the CD signal being maximized by optimizing this angle and locking the two naphthalene units in a rigid structure. Additionally, in the CD spectra, the end groups, present at wavelengths below 300 nm, remain visible before and after aggregation. This signal originates from one of the two naphthalene units angled relative to the one in conjugation with the rest of the polymer

https://doi.org/10.1021/acs.macromol.4c02054
Macromolecules 2024, 57, 11229−11241

backbone. Under poor solvent conditions, this naphthalene is not in conjugation with the rest of the polymer backbone, thereby preventing the signal below 300 nm from fully disappearing. To compare the strength of the chiral expression in the first series of polymers, the $g_{abs,max}$ ($=\Delta\varepsilon/\varepsilon$) values are determined (Table 2). For **STILB GALL*-P3OT$_{30}$**, no $g_{abs,max}$ can be determined due to the absence of a CD signal. For **STILB HQ*-P3OT$_{28}$** and **BINOL 2xMe*-P3OT$_{33}$**, these $g_{abs,max}$ values are in the order of 10^{-4}. For **BINOL P* P3OT$_{33}$** and **BINOL M* P3OT$_{39}$**, this value increases nearly 1 order of magnitude, further demonstrating that the polymers with propylene- and methylene-linked BINOL end groups are more effective at inducing chiral expression. These polymer samples are also measured in thin films to confirm that the chiral expression resulting from supramolecular organization is not restricted to aggregates in solution. The results align with the measurements in solution: polymers with BINOL-derived end groups again exhibit the strongest chiral expression ($g_{abs,max}$ values $\approx 10^{-4}$). For the stilbene-derived end groups, **STILB HQ*-P3OT$_{28}$** shows a CD signal, though it is very weak ($g_{abs,max} < 10^{-5}$), while **STILB GALL*-P3OT$_{30}$** does not display any chiral expression (Supporting Information, Part 9b–d). Overall, the $g_{abs,max}$ values decrease, and the sign of the CD signal reverses compared to aggregation in solution. This difference arises from the methods used to form the aggregates. Film formation is a very rapid process, while solvatochromism experiments generally require longer time scales. Consequently, the supramolecular aggregates follow distinct formation pathways, which impact their chiral expression.

Table 2. Values for the $g_{abs,max}$ ($=\Delta\varepsilon/\varepsilon$) for the First Series of Polymers Based on UV–Vis and CD Spectra[a]

Polymer	$g_{abs,max}$
STILB GALL*-P3OT$_{30}$	
STILB HQ*-P3OT$_{28}$	$2.0 \pm 0.2 \times 10^{-4}$
BINOL P* P3OT$_{33}$	$9.7 \pm 0.4 \times 10^{-4}$
BINOL M* P3OT$_{39}$	$1.0 \pm 0.1 \times 10^{-3}$
BINOL 2xMe* P3OT$_{33}$	$1.5 \pm 0.2 \times 10^{-4}$
STILB HQ* P3OT$_{25}$	$4.8 \pm 1.3 \times 10^{-4}$
STILB HQ* P3OT$_{23}$	$5.7 \pm 0.5 \times 10^{-4}$

[a]**STILB GALL*-P3OT$_{30}$** has no values due to the absence of a CD signal.

It is also anticipated that the DP influences the chiral expression when these chiral end groups are used. To test this, two additional hydroquinone-based stilbene-initiated polymers are synthesized, in addition to **STILB HQ*-P3OT$_{28}$**, with slight variations in DP. As is shown in Table 1, **STILB HQ* P3OT$_{25}$** has a DP of 25 and **STILB HQ* P3OT$_{23}$** has a DP of 23, as determined by ^{1}H NMR. They both have SEC-to-^{1}H NMR molar mass ratios similar to **STILB HQ*-P3OT$_{28}$**, with the ratio of **STILB HQ* P3OT$_{23}$** being slightly lower, possibly attributed to its lower DP, which also affects the overestimation. Upon aggregation, both samples exhibit chiral expression, with the sample having the lowest DP showing the strongest chiral expression (Figure 4). The $g_{abs,max}$ values confirm this. **STILB HQ* P3OT$_{23}$**, **STILB HQ* P3OT$_{25}$**, and **STILB HQ*-P3OT$_{28}$**, increasing in DP, show respective values of 6×10^{-4}, 5×10^{-4}, and 2×10^{-4}. This demonstrates that as the DP increases, the relative contribution of the end group to the overall polymer chain decreases, reducing the chiral expression. Despite the limited differences in DP, the influence on chiral expression is significant, indicating that maintaining a low DP is essential for maximizing chiral expression. This further supports that BINOL end groups are able to express a stronger chiral response, as their DPs were consistently higher compared with the stilbene counterparts.

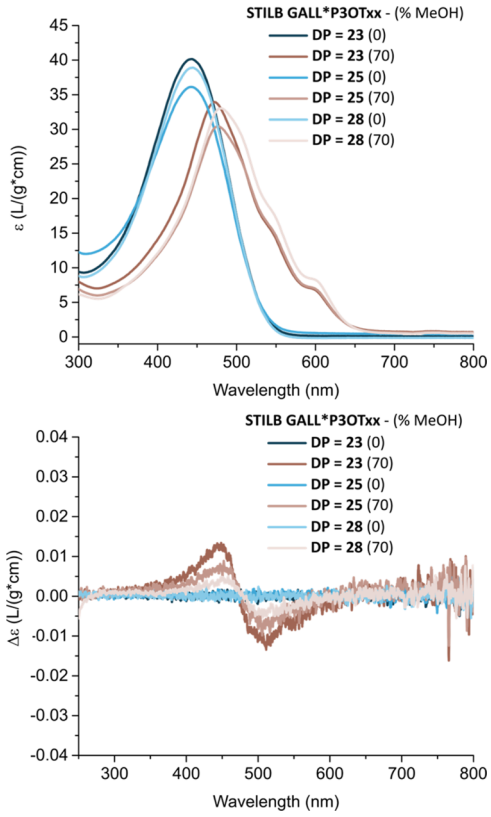

Figure 4. Absorption and CD spectra of the solvatochromism experiments investigating a difference in DP. The blue spectra are samples measured in $CHCl_3$, whereas the brown spectra are under poor solvent conditions (70% MeOH).

Finally, in a second series, the interaction between the (chiral) end group and the chiral P3AT is explored. Specifically, the potential of an achiral or chiral end group to influence or hinder chiral aggregation using chiral monomers is investigated. External initiators **4a** or **13a** (chiral) and **4b** or **13b** (achiral) are used in combination with achiral **M1** or chiral (*S*)-2-(5-bromo-4-(3,7-dimethyloctyl)thiophen-2-yl)-4,4,5,5-tetramethyl-1,3,2-dioxaborolane **M2** (Scheme 4 and Supporting Information, Part 3). As shown in Table 3 and visualized in Figure 5, six additional polymers are synthesized alongside the previously synthesized **STILB GALL*-P3OT$_{30}$** and **STILB HQ*-P3OT$_{28}$**. It is important to note that this approach does not apply to the BINOL derivatives due to their inherent axial chirality, which precludes the possibility of creating an achiral BINOL derivative. The alternative would be to synthesize and use the racemic equivalent to replace the abundantly available (*S*)-enantiomer. However, combining this end group with chiral monomers would result in diastereomers, unnecessarily complicating the aggregation behavior.

Based on SEC, MALDI-ToF, and ^{1}H NMR data, the $\bar{M}_n$ and DP of the other 3 **STILB GALL$^{(*)}$** (chiral or achiral) based polymers, **STILB GALL*-P3OT*$_{31}$**, **STILB GALL-P3OT*$_{32}$**, and **STILB GALL-P3OT$_{28}$**, are consistent with those of **STILB GALL*-P3OT$_{30}$**. The higher molar masses of **STILB GALL*-P3OT*$_{31}$** and **STILB GALL-P3OT*$_{32}$** can be

https://doi.org/10.1021/acs.macromol.4c02054
Macromolecules 2024, 57, 11229–11241

Scheme 4. Overview of the SMCTCP of Achiral M1 or Chiral M2 in Combination with Chiral (4a and 13a) and Achiral (4b and 13b) Stilbene-Derived External Initiators[a]

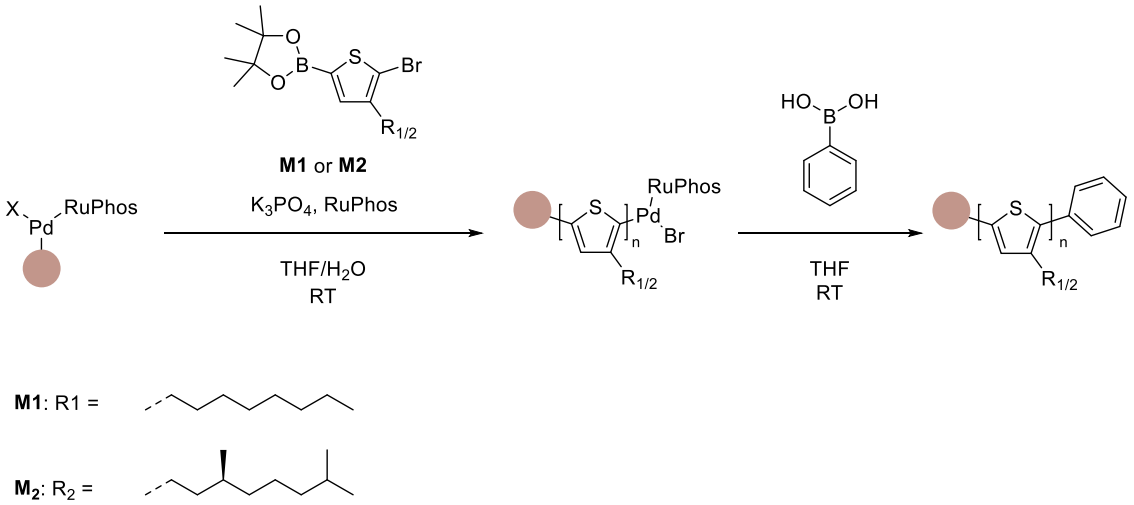

[a]With "brown circle solid" being the chiral or achiral stilbene-derived aromatic compounds. RuPhos = 2-dicyclohexylphosphino-2′,6′-di*iso*propoxybiphenyl.

Table 3. Overview of the SMCTCP of M1 (Chiral) and M2 (Achiral) Using Chiral External Initiators (4a and 13a) and Achiral External Initiators (4b and 13b)[a]

polymer	Pd initiator	monomer	M/I	time	$\bar{M}_n$[b]	$Đ$[b]	DP	MM[c] (kg/mol)	$\frac{\bar{M}_n}{MM}$[c]
STILB GALL*-P3OT$_{30}$	**4a**	**M1**	30	21 h	8.7	1.25	30	6.3	1.38
STILB GALL*-P3OT*$_{31}$	**4a**	**M2**	30	21 h	8.8	1.20	31	7.3	1.21
STILB GALL-P3OT*$_{32}$	**4b**	**M2**	30	21 h	8.8	1.21	32	7.5	1.17
STILB GALL-P3OT$_{28}$	**4b**	**M1**	30	5 h 30	7.6	1.19	28	5.8	1.31
STILB HQ*-P3OT$_{28}$	**13a**	**M1**	30	6 h	7.2	1.23	28	6.0	1.20
STILB HQ*-P3OT*$_{30}$	**13a**	**M2**	30	3 h 30	7.6	1.19	30	7.2	1.06
STILB HQ-P3OT*$_{29}$	**13b**	**M2**	30	4 h	7.5	1.21	29	6.9	1.09
STILB HQ-P3OT$_{28}$	**13b**	**M1**	30	4 h	7.2	1.23	28	5.9	1.22

[a]M/I: monomer-to-initiator ratio used to determine the theoretical DP. [b]$\bar{M}_n$ and $Đ$ are determined via SEC measurements. [c]DP and MM (molar mass) are determined via ^{1}H NMR.

attributed to the higher molar mass of chiral **M2** compared to the achiral equivalent **M1**. The dispersity of all three samples ranges between 1.19 and 1.21, which is consistent as well. Similar observations are made for polymers with a **STILB HQ(*)** (chiral or achiral)-based end group, **STILB HQ*-P3OT*$_{30}$**, **STILB HQ-P3OT*$_{29}$**, and **STILB HQ-P3OT$_{28}$**. SEC-to-^{1}H NMR molar mass ratios differ notably in these polymer series. Polymers with chiral monomers have ratios lower than those with achiral monomers. Specifically, chiral monomer-based polymers **STILB GALL*-P3OT$_{30}$** and **STILB GALL-P3OT$_{28}$** have a ratio of 1.38 and 1.31, respectively, while **STILB GALL*-P3OT*$_{31}$** and **STILB GALL-P3OT*$_{32}$**, based on achiral monomers, have ratios at or below 1.21. A similar trend is observed for **STILB HQ*-P3OT$_{28}$** and **STILB HQ-P3OT$_{28}$**, which have ratios at or above 1.20, higher than those of **STILB HQ*-P3OT*$_{30}$** and **STILB HQ-P3OT*$_{29}$**, which are below 1.10. This difference is expected, as the branched C10 side chain of the chiral monomer offers more flexibility compared with the linear C8 side chain in the achiral monomer, leading to a smaller hydrodynamic volume compared to their molar mass.

During aggregation, both series, **STILB GALL(*)** or **STILB HQ(*)** based, yield comparable results under good solvent conditions. As previously mentioned, **STILB GALL*-P3OT$_{30}$** does not aggregate in a chiral manner under poorer solvent conditions. However, when the monomer is switched from achiral **M1** to chiral **M2**, as in **STILB GALL*-P3OT*$_{31}$**, a CD signal appears (Figure 6a). Likewise, in **STILB GALL-P3OT*$_{32}$**, where an achiral end group is combined with chiral **M2**, a CD signal similar to that of **STILB GALL*-P3OT*$_{31}$** is observed. This again confirms that the end group, with its side chains perpendicular to the polymer side chain, cannot steer or influence the aggregation behavior. For **STILB HQ*-P3OT$_{28}$**, a small negative CD signal is obtained under 70% MeOH conditions. **STILB HQ*-P3OT*$_{30}$**, which combines a chiral end group with a chiral polymer backbone, also exhibits chiral expression (Figure 6b). However, the sign of the CD signal changes compared to **STILB HQ*-P3OT$_{28}$** and the intensity increases. A similar result is obtained for **STILB HQ-P3OT*$_{29}$**, which consists of an achiral end group with a chiral polymer backbone, indicating that the end group does not hinder or influence the stacking behavior of a polymer backbone made from chiral monomers. In Table 4, the $g_{abs,max}$ values of these polymers are compared. For both stilbene end groups, a clear trend is observed. The polymers using chiral monomer **M2** have a $g_{abs,max}$ of 10^{-3}, which is an order of magnitude larger compared to that of the **STILB HQ*-P3OT$_{28}$**.

https://doi.org/10.1021/acs.macromol.4c02054
Macromolecules 2024, 57, 11229−11241

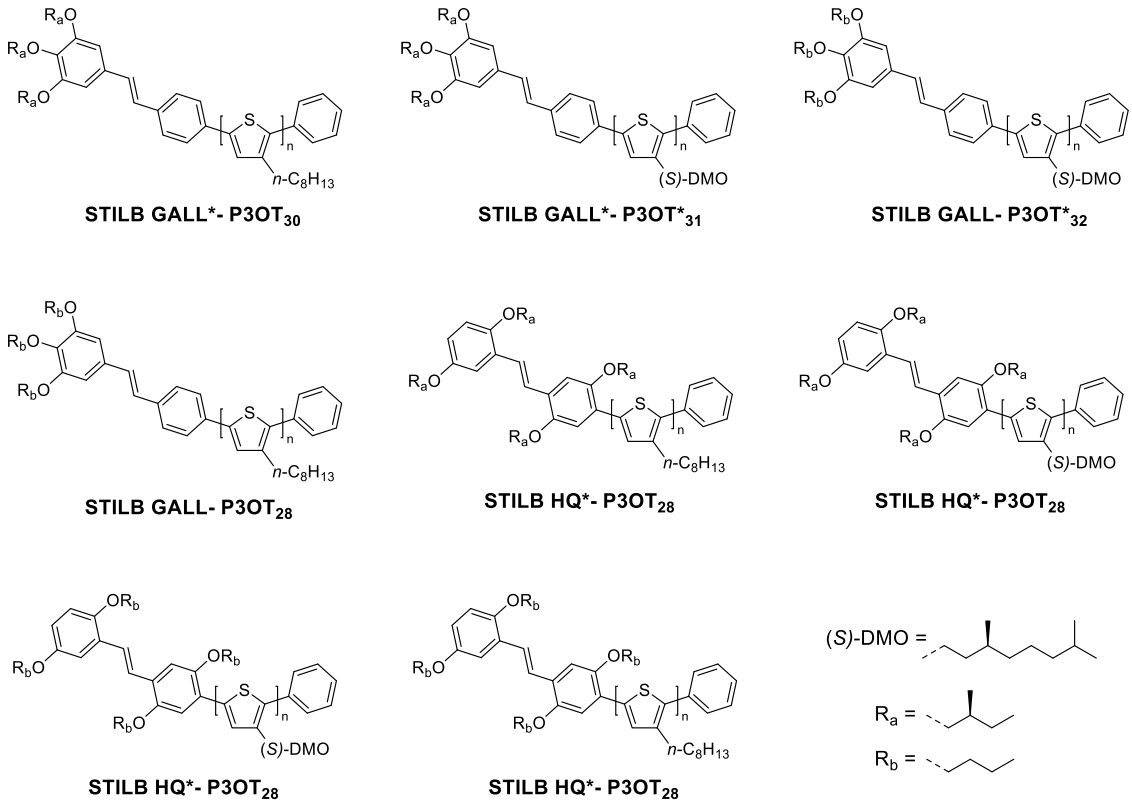

Figure 5. Overview of the second series of polymers. With $R_{a/b}$ being the side chains of the end group and (S)-DMO being the chiral (*S*)-3,7-dimethyloctyl side chain.

Overall, the **STILB HQ*** end group can be used to induce chirality in P3OT, although its chiral expression is less pronounced compared with polymers synthesized entirely from chiral monomers. The lower $g_{abs,max}$ from **STILB HQ*-P3OT$_{28}$** occurs due to the limited "density" of the chiral centra in the polymer structure. It has one chiral end group on approximately 30 achiral monomers versus approximately 30 chiral monomers in **STILB HQ$^{(*)}$-P3OT*$_{xx}$**. For comparison, these materials should also be evaluated with previously synthesized chiral copolymers with a lower chiral density, such as the random copolymer poly((3-octylthiophene)-*co*-(2-(*S*)-methylbutyl)thiophene) (**P3OT$_{27}$-*co*-3BT*$_9$**). This CP consists of two thiophene monomers: one with an (*S*)-2-methylbutyl side chain, similar to the side chains of the end group and the other one being the achiral 3-octylthiophene.[30] In this **P3OT$_{27}$-*co*-3BT*$_9$**, the lowest chiral density originating from the **3BT*** is 25%, calculated by dividing the number of chiral side chains by the total number of side chains. In **STILB HQ*-P3OT$_{28}$**, the chiral density is 12%. For **P3OT-*co*-3BT***, the $g_{abs,max}$ is in the order of 10^{-4}, which is similar to the $g_{abs,max}$ of **STILB HQ*-P3OT$_{28}$**. However, **BINOL M* P3OT$_{39}$**, with a $g_{abs,max}$ in the order of 10^{-3} and a chiral density of only 3%, exhibits a chiral expression 10 times stronger, demonstrating that these end groups efficiently introduce chirality in P3OT.

CONCLUSIONS

The impact and potential of chiral end groups for inducing chiral expression in achiral P3OTs were investigated through the synthesis and isolation of two different types of external initiators. The external initiators efficiently introduce chiral end groups at the beginning of the CPs. The first type is stilbene derivatives with a stereogenic carbon atom in their side chains. The position and orientation relative to the side chains of the CP are critical, i.e., the side chains need to be relatively close and parallel to the side chains of the CP in order to induce chiral expression in achiral P3OT ($g_{abs,max}$ = 10^{-4}). Additionally, the DP influences the intensity of the CD signal. The higher the DP, the smaller the share of the end group, reducing its impact on the chiral expression and resulting in a smaller CD signal. The second type of external initiator is based on (*S*)-(−)-1,1′-bi(2-naphthol), which possesses axial chirality without the presence of stereogenic carbon atoms. The dihedral angle was altered by linking the two naphthol units with two different spacers or remaining unlinked. These linkers also influence the rigidity and bulkiness of the end group. A more rigid structure, obtained using the linkers, results in stronger chiral expression ($g_{abs,max}$ = 10^{-3}) under aggregated conditions compared to P3OT with an unlinked BINOL end group ($g_{abs,max}$ = 10^{-4}). Changing the length and nature of the linker, which impacts the dihedral angle, also influences the intensity of the chiral signal to some extent.

When chiral monomers are used in combination with the different chiral end groups, the end groups are no longer dominant during aggregation and the chiral polymer backbone dictates the self-assembly of the CPs. Depending on the chiral end group, the $g_{abs,max}$ values of fully chiral polymers are typically 5 to 20 times stronger than those of polymers where the end group is the only chiral entity. However, when considering chiral density, the linked BINOL-derived polymers (**BINOL M* P3OT$_{39}$** and **BINOL P* P3OT$_{33}$**) with a chiral density of 3% surpass the $g_{abs,max}$ of a copolymer such as **P3OT-*co*-3BT***, which has a chiral density of 22%, demonstrating the efficiency of this system. In conclusion, a new method for introducing chiral expression based on the

https://doi.org/10.1021/acs.macromol.4c02054
Macromolecules 2024, 57, 11229−11241

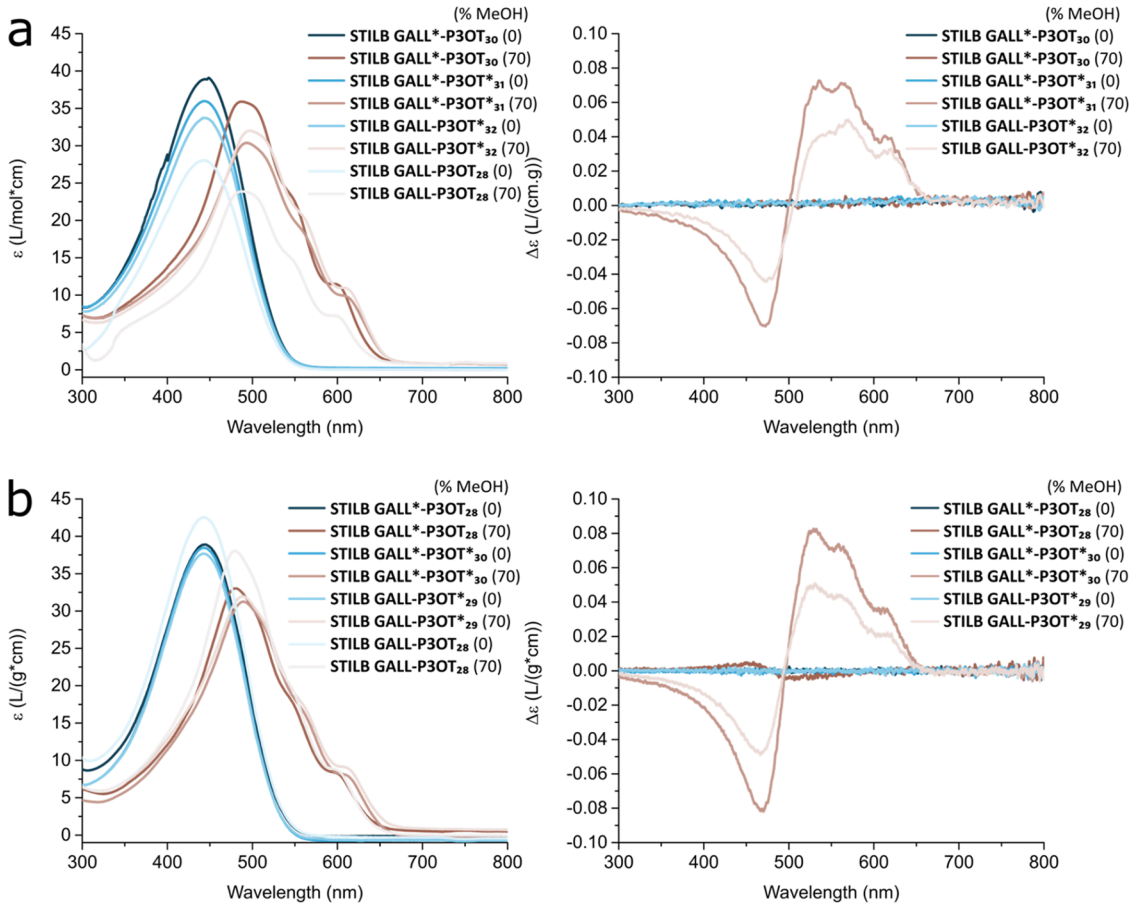

Figure 6. Absorption and CD spectra of the solvatochromism experiments investigating the influence of the end group on the aggregation behavior of (a) polymers with a stilbene end group based on a gallate derivative and (b) polymers with a stilbene end group based on a hydroquinone derivative. The blue spectra are samples measured in $CHCl_3$, whereas the brown spectra are under diminished solvent conditions (70% MeOH).

Table 4. Values for the $g_{abs,max}$ ($=\Delta\varepsilon/\varepsilon$) for the Second Series of Polymers Based on UV–Vis and CD Spectra[a]

polymer	$g_{abs,max}$
STILB GALL*-P3OT$_{30}$	
STILB GALL*-P3OT*$_{31}$	$4.5 \pm 0.1 \times 10^{-3}$
STILB GALL-P3OT*$_{32}$	$3.8 \pm 0.1 \times 10^{-3}$
STILB GALL-P3OT$_{28}$	
STILB HQ*-P3OT$_{28}$	$2.0 \pm 0.2 \times 10^{-4}$
STILB HQ*-P3OT*$_{30}$	$4.9 \pm 0.1 \times 10^{-3}$
STILB HQ-P3OT*$_{29}$	$2.8 \pm 0.1 \times 10^{-3}$
STILB HQ-P3OT$_{28}$	

[a]**STILB GALL*-P3OT$_{30}$** has no values due to the absence of a CD signal. **STILB GALL-P3OT$_{28}$** and **STILB HQ-P3OT$_{28}$** do not have values as they are achiral.

sergeants and soldiers principle in seemingly achiral P3OTs is developed through the efficient implementation of sterically bulky or strongly aggregating chiral end groups.

■ ASSOCIATED CONTENT

Supporting Information

The Supporting Information is available free of charge at https://pubs.acs.org/doi/10.1021/acs.macromol.4c02054.

Materials; instrumentation; synthetic procedures; ^{1}H NMR spectra, SEC elution graphs of the synthesized polymers, MALDI-ToF spectra, and UV–vis and CD spectra (PDF)

■ AUTHOR INFORMATION

Corresponding Author

Guy Koeckelberghs − *Laboratory for Polymer Synthesis, KU Leuven, B-3001 Heverlee, Belgium;* Present Address: Laboratory for Polymer Synthesis, KU Leuven, Celestijnenlaan 200F, B-3001 Heverlee, Belgium; orcid.org/0000-0003-1412-8454; Email: guy.koeckelberghs@kuleuven.be

Authors

Siebe Detavernier − *Laboratory for Polymer Synthesis, KU Leuven, B-3001 Heverlee, Belgium;* Present Address: Laboratory for Polymer Synthesis, KU Leuven, Celestijnenlaan 200F, B-3001 Heverlee, Belgium

Trijntje Paredis − *Laboratory for Polymer Synthesis, KU Leuven, B-3001 Heverlee, Belgium;* Present Address: Laboratory for Polymer Synthesis, KU Leuven, Celestijnenlaan 200F, B-3001 Heverlee, Belgium

Silvia Pratesi − *Laboratory for Polymer Synthesis, KU Leuven, B-3001 Heverlee, Belgium;* Present Address: Laboratory for Polymer Synthesis, KU Leuven, Celestijnenlaan 200F, B-3001 Heverlee, Belgium; Present Address: Department of Industrial Chemistry, "Toso Montanari", Viale del Risorgimento 4, 40136 Bologna, Italy.

Julien De Winter − *Laboratory for Polymer Synthesis, KU Leuven, B-3001 Heverlee, Belgium;* Present Address: Organic Synthesis and Mass Spectrometry Laboratory, Center of Innovation and Research in

https://doi.org/10.1021/acs.macromol.4c02054
Macromolecules 2024, 57, 11229−11241

Materials and Polymers (CIRMAP)—University of Mons (UMONS), Place du Parc 23, B-7000 Mons, Belgium.; orcid.org/0000-0003-3429-5911

Elisabetta Salatelli − *Laboratory for Polymer Synthesis, KU Leuven, B-3001 Heverlee, Belgium;* Present Address: Department of Industrial Chemistry, "Toso Montanari", Viale del Risorgimento 4, 40136 Bologna, Italy.

Pascal Gerbaux − *Laboratory for Polymer Synthesis, KU Leuven, B-3001 Heverlee, Belgium;* Present Address: Organic Synthesis and Mass Spectrometry Laboratory, Center of Innovation and Research in Materials and Polymers (CIRMAP)—University of Mons (UMONS), Place du Parc 23, B-7000 Mons, Belgium.; orcid.org/0000-0001-5114-4352

Complete contact information is available at: https://pubs.acs.org/10.1021/acs.macromol.4c02054

Author Contributions

All authors have given approval to the final version of the manuscript. All authors significantly contributed to this research. S.D., T.P., and S.P. were the main contributors to the investigation, methodology, and validation. S.D. conducted the visualization and writing of the original draft. P.G. and J.D.W. were responsible for the formal analysis and investigation of MALDI-ToF data. E.S. was responsible for proofreading the original draft. G.K. was responsible for conceptualization, funding acquisition, project administration, and supervision. All contributed evenly to the review and editing of writing this manuscript.

Funding

Funding sources-1SB1623N Infrastructure grant I002720N.

Notes

The authors declare no competing financial interest.

■ ACKNOWLEDGMENTS

This research was funded by the Fund for Scientific Research (FWO-Flanders-1SB1623N) and by Onderzoeksfonds KU Leuven/Research Fund KU Leuven. S.D. is a doctoral fellow of the Fund for Scientific Research (FWO-Flanders). This research was supported by the Research Foundation Flanders (FWO) through infrastructure grant I002720N. The authors acknowledge the use of ChatGPT to identify improvements in the writing style.

■ ABBREVIATIONS

BINOL, (*S*)-(−)-1,1′-bi(2-naphthol); CD, circular dichroism; $CHCl_3$, chloroform; CP, conjugated polymer; dba, dibenzylideneacetone; DP, degree of polymerization; HOMO, highest occupied molecular orbital; LUMO, lowest unoccupied molecular orbital; MALDI-ToF, matrix-assisted laser desorption/ionization-time-of-flight; MeOH, methanol; $\bar{M}_n$, number-average molar mass; $NABH_4$, sodium borohydride; oFETs, organic field-effect transistors; oLEDs, organic light-emitting diodes; oPVs, organic photovoltaics; P3AT, poly(3-alkylthiophene); P3DMOT, poly(3-(3,7-(*S*)-dimethyloctylthiophene)); P3OT, poly(3-octylthiophene); SEC, size-exclusion chromatography; SMCTCP, Suzuki−Miyaura catalyst transfer condensative polymerization; $SOCl_2$, thionyl chloride; TE, thermo-electrics

■ REFERENCES

(1) Facchetti, A. π-Conjugated Polymers for Organic Electronics and Photovoltaic Cell Applications. *Chem. Mater.* **2011**, *23* (3), 733−758.
(2) Usta, H.; Facchetti, A.; Marks, T. J. N-Channel Semiconductor Materials Design for Organic Complementary Circuits. *Acc. Chem. Res.* **2011**, *44* (7), 501−510.
(3) Feng, X.; Lv, F.; Liu, L.; Tang, H.; Xing, C.; Yang, Q.; Wang, S. Conjugated Polymer Nanoparticles for Drug Delivery and Imaging. *ACS Appl. Mater. Interfaces* **2010**, *2* (8), 2429−2435.
(4) Beaujuge, P. M.; Fréchet, J. M. J. Molecular Design and Ordering Effects in π-Functional Materials for Transistor and Solar Cell Applications. *J. Am. Chem. Soc.* **2011**, *133* (50), 20009−20029.
(5) Baker, M. A.; Tsai, C. H.; Noonan, K. J. T. Diversifying Cross-Coupling Strategies, Catalysts and Monomers for the Controlled Synthesis of Conjugated Polymers. *Chem. - Eur. J.* **2018**, *24* (50), 13078−13088.
(6) Nguyen, T. N.; Phung, V. D.; van Tran, V. Recent Advances in Conjugated Polymer-Based Biosensors for Virus Detection. *Biosensors* **2023**, *13* (6), 586.
(7) Wang, C.; Dong, H.; Hu, W.; Liu, Y.; Zhu, D. Semiconducting π-Conjugated Systems in Field-Effect Transistors: A Material Odyssey of Organic Electronics. *Chem. Rev.* **2012**, *112* (4), 2208−2267.
(8) Wang, S.; Zuo, G.; Kim, J.; Sirringhaus, H. Progress of Conjugated Polymers as Emerging Thermoelectric Materials. *Prog. Polym. Sci.* **2022**, *129*, No. 101548.
(9) Hoeben, F. J. M.; Jonkheijm, P.; Meijer, E. W.; Schenning, A. P. H. J. About Supramolecular Assemblies of π-Conjugated Systems. *Chem. Rev.* **2005**, *105* (4), 1491−1546.
(10) Sirringhaus, H.; Brown, P. J.; Friend, R. H.; Nielsen, M. M.; Bechgaard, K.; Langeveld-Voss, B. M. W.; Spiering, A. J. H.; Janssen, R. A. J.; Meijer, E. W.; Herwig, P.; De Leeuw, D. M. Two-Dimensional Charge Transport in Self-Organized, High-Mobility Conjugated Polymers. *Nature* **1999**, *401* (6754), 685−688.
(11) Kline, J. R.; McGehee, M. D.; Kadnikova, E. N.; Liu, J.; J FrØchet, J. M.; McGehee, M. D.; Kline, R. J.; Kadnikova, E. N.; Liu, J.; J Fréchet, J. M. Controlling the Field-Effect Mobility of Regioregular Polythiophene by Changing the Molecular Weight. *Adv. Mater.* **2003**, *15* (18), 1519−1522.
(12) Noriega, R.; Rivnay, J.; Vandewal, K.; Koch, F. P. V.; Stingelin, N.; Smith, P.; Toney, M. F.; Salleo, A. A General Relationship between Disorder, Aggregation and Charge Transport in Conjugated Polymers. *Nat. Mater.* **2013**, *12* (11), 1038−1044.
(13) Willot, P.; Steverlynck, J.; Moerman, D.; Leclère, P.; Lazzaroni, R.; Koeckelberghs, G. Poly(3-Alkylthiophene) with Tuneable Regioregularity: Synthesis and Self-Assembling Properties. *Polym. Chem.* **2013**, *4* (9), 2662−2671.
(14) Peeters, H.; Couturon, P.; Vandeleene, S.; Moerman, D.; Leclère, P.; Lazzaroni, R.; Cat, I. De.; Feyter, S. De.; Koeckelberghs, G. Influence of the Regioregularity on the Chiral Supramolecular Organization of Poly(3-Alkylsulfanylthiophene)s. *RSC Adv.* **2013**, *3* (10), 3342−3351.
(15) Verheyen, L.; De Winter, J.; Gerbaux, P.; Koeckelberghs, G. Effect of the Nature and the Position of Defects on the Chiral Expression in Poly(3-Alkylthiophene)s. *Macromolecules* **2019**, *52* (22), 8587−8595.
(16) Prosa, T. J.; Winokur, M. J.; McCullough, R. D. Evidence of a Novel Side Chain Structure in Regioregular Poly(3-Alkylthiophenes). *Macromolecules* **1996**, *29* (10), 3654−3656.
(17) Meille, S. V.; Romita, V.; Caronna, T.; Lovinger, A. J.; Catellani, M.; Belobrzeckaja, L. Influence of Molecular Weight and Regioregularity on the Polymorphic Behavior of Poly(3-Decylthiophenes). *Macromolecules* **1997**, *30* (25), 7898−7905.
(18) Bridges, C. R.; Ford, M. J.; Thomas, E. M.; Gomez, C.; Bazan, G. C.; Segalman, R. A. Effects of Side Chain Branch Point on Self Assembly, Structure, and Electronic Properties of High Mobility Semiconducting Polymers. *Macromolecules* **2018**, *51* (21), 8597−8604.
(19) Van Oosten, A.; Verduyckt, C.; De Winter, J.; Gerbaux, P.; Koeckelberghs, G. Influence of the Dispersity and Molar Mass

Distribution of Conjugated Polymers on the Aggregation Type and Subsequent Chiral Expression. *Soft Matter* **2023**, *19* (21), 3794−3802.
(20) Tsao, H. N.; Cho, D.; Andreasen, J. W.; Rouhanipour, A.; Breiby, D. W.; Pisula, W.; Müllen, K. The Influence of Morphology on High-Performance Polymer Field-Effect Transistors. *Adv. Mater.* **2009**, *21* (2), 209−212.
(21) Wang, Y.; Cui, H.; Zhu, M.; Qiu, F.; Peng, J.; Lin, Z. Tailoring Phase Transition in Poly(3-Hexylselenophene) Thin Films and Correlating Their Crystalline Polymorphs with Charge Transport Properties for Organic Field-Effect Transistors. *Macromolecules* **2017**, *50* (24), 9674−9682.
(22) Brinkmann, M. Structure and Morphology Control in Thin Films of Regioregular Poly(3-Hexylthiophene). *J. Polym. Sci., Part B:Polym. Phys.* **2011**, *49* (17), 1218−1233.
(23) Koldemir, U.; Puniredd, S. R.; Wagner, M.; Tongay, S.; McCarley, T. D.; Kamenov, G. D.; Müllen, K.; Pisula, W.; Reynolds, J. R. End Capping Does Matter: Enhanced Order and Charge Transport in Conjugated Donor-Acceptor Polymers. *Macromolecules* **2015**, *48* (18), 6369−6377.
(24) Van Oosten, A.; Verduyckt, C.; Koeckelberghs, G. Introducing Molecular Asymmetry in Copolymer Structures to Favor Herringbone-Like Aggregation and Tune the Chiral Expression. *Macromolecules* **2023**, *56* (19), 7698−7706.
(25) Van Den Eede, M. P.; Van Gestel, L.; Koeckelberghs, G. Expression of Chirality in Tailor-Made Conjugated Polymers. *Macromolecules* **2018**, *51* (17), 6602−6608.
(26) Van Den Eede, M. P.; Bedi, A.; Delabie, J.; De Winter, J.; Gerbaux, P.; Koeckelberghs, G. The Influence of the End-Group on the Chiral Self-Assembly of All-Conjugated Block Copolymers. *Polym. Chem.* **2017**, *8* (37), 5666−5672.
(27) Ishidate, R.; Markvoort, A. J.; Maeda, K.; Yashima, E. Unexpectedly Strong Chiral Amplification of Chiral/Achiral and Chiral/Chiral Copolymers of Biphenylylacetylenes and Further Enhancement/Inversion and Memory of the Macromolecular Helicity. *J. Am. Chem. Soc.* **2019**, *141* (18), 7605−7614.
(28) Green, M. M.; Reidy, M. P.; Johnson, R. J.; Darling, G.; O'Leary, D. J.; Willson, G. Macromolecular Stereochemistry: The Out-of-Proportion Influence of Optically Active Comonomers on the Conformational Characteristics of Polyisocyanates. The Sergeants and Soldiers Experiment. *J. Am. Chem. Soc.* **1989**, *111* (16), 6452−6454.
(29) Langeveld-Voss, B. M. W.; Waterval, R. J. M.; Janssen, R. A. J.; Meijer, E. W. Principles of 'majority Rules' and 'sergeants and Soldiers' Applied to the Aggregation of Optically Active Polythiophenes: Evidence for a Multichain Phenomenon. *Macromolecules* **1999**, *32* (1), 227−230.
(30) Verswyvel, M.; Monnaie, F.; Koeckelberghs, G. AB Block Copoly(3-Alkylthiophenes): Synthesis and Chiroptical Behavior. *Macromolecules* **2011**, *44* (24), 9489−9498.
(31) Willot, P.; Koeckelberghs, G. Evidence for Catalyst Association in the Catalyst Transfer Polymerization of Thieno[3,2- b]Thiophene. *Macromolecules* **2014**, *47* (24), 8548−8555.
(32) Hannigan, M. D.; Tami, J. L.; Zimmerman, P. M.; McNeil, A. J. Rethinking Catalyst Trapping in Ni-Catalyzed Thieno[3,2- b]-Thiophene Polymerization. *Macromolecules* **2022**, *55* (24), 10821−10830.
(33) Sugita, H.; Kamigawara, T.; Miyazaki, S.; Shimada, R.; Katoh, T.; Ohta, Y.; Yokozawa, T. Intramolecular Palladium Catalyst Transfer on Benzoheterodiazoles as Acceptor Monomers and Discovery of Catalyst Transfer Inhibitors. *Chem. - Eur. J.* **2023**, *29* (47), No. e202301242.
(34) Seo, K. B.; Lee, I. H.; Lee, J.; Choi, I.; Choi, T. L. A Rational Design of Highly Controlled Suzuki-Miyaura Catalyst-Transfer Polycondensation for Precision Synthesis of Polythiophenes and Their Block Copolymers: Marriage of Palladacycle Precatalysts with MIDA-Boronates. *J. Am. Chem. Soc.* **2018**, *140* (12), 4335−4343.
(35) Kim, H.; Lee, J.; Kim, T.; Cho, M.; Choi, T. L. Precision Synthesis of Various Low-Bandgap Donor−Acceptor Alternating Conjugated Polymers via Living Suzuki−Miyaura Catalyst-Transfer Polymerization. *Angew. Chem., Int. Ed.* **2022**, *61* (31), No. e202205828.
(36) Lee, J.; Park, H.; Hwang, S.-H.; Lee, I.-H.; Choi, T.-L. RuPhos Pd Precatalyst and MIDA Boronate as an Effective Combination for the Precision Synthesis of Poly(3-Hexylthiophene): Systematic Investigation of the Effects of Boronates, Halides, and Ligands. *Macromolecules* **2020**, *53* (9), 3306−3314.
(37) Lee, J.; Kim, H.; Park, H.; Kim, T.; Hwang, S. H.; Seo, D.; Chung, T. D.; Choi, T. L. Universal Suzuki-Miyaura Catalyst-Transfer Polymerization for Precision Synthesis of Strong Donor/Acceptor-Based Conjugated Polymers and Their Sequence Engineering. *J. Am. Chem. Soc.* **2021**, *143* (29), 11180−11190.
(38) Monga Mulunda, M.; van Goethem, C.; Zhang, Z.; Nies, E.; Vankelecom, I.; Koeckelberghs, G. Influence of the Molecular Structure of Polybinaphthalene on the Membrane Separation Performance. *Eur. Polym. J.* **2018**, *101*, 248−254.
(39) Dujardin, W.; Van Goethem, C.; Zhang, Z.; Verbeke, R.; Dickmann, M.; Egger, W.; Nies, E.; Vankelecom, I.; Koeckelberghs, G. Fine-Tuning the Molecular Structure of Binaphthalene Polyimides for Gas Separations. *Eur. Polym. J.* **2019**, *114*, 134−143.
(40) Nojima, M.; Ohta, Y.; Yokozawa, T. Structural Requirements for Palladium Catalyst Transfer on a Carbon-Carbon Double Bond. *J. Am. Chem. Soc.* **2015**, *137* (17), 5682−5685.

https://doi.org/10.1021/acs.macromol.4c02054
Macromolecules 2024, 57, 11229−11241